Active mitigation of self-excited vibrations of a magnetic track brake

Journal of Physics: Conference Series **2647** (2024) 152007 doi:10.1088/1742-6596/2647/15/152007

Active mitigation of self-excited vibrations of a magnetic track brake

Bernhard Ebner[1], Daniel Tippelt[2], Johannes Edelmann[1], and Manfred Plöchl[3]

[1] Christian Doppler Laboratory for Enhanced Braking Behaviour of Railway Vehicles, Institute of Mechanics and Mechatronics, TU Wien, Vienna, Austria
[2] Knorr-Bremse GmbH, Mödling, Austria
[3] Institute of Mechanics and Mechatronics, TU Wien, Vienna, Austria

E-mail: bernhard.ebner@tuwien.ac.at

Abstract. Magnetic track brakes (*mtb*s) are additional braking systems used in railway vehicles at emergency situations and low adhesion conditions. Operation at low velocities can cause harmful self-excited vibrations, which must be avoided at all circumstances. Few passive countermeasures are already published, but active vibration control of an *mtb* lacks in literature so far. In this paper an active vibration control to diminish self-excited vibrations, based on reducing the energy, drawn by the oscillating system, is studied. Considering a minimal model of the *mtb*, the energy input depends on the electromagnetic-mechanical coupling and the friction force in the *mtb*—rail contact. The obtained equation of this energy reveal a dependency of the phase shift, between magnetic flux and the oscillatory mechanical motion. A control law for the input voltage is obtained to reach a specific phase shift reducing the energy input and oscillating amplitudes.

1. Introduction

Magnetic track brakes (*mtb*s) are additional braking systems used in railway vehicles at emergency situations and low adhesion conditions. They operate independent from the wheel–rail contact and provide braking forces in addition to brakes on the wheelset to meet obligatory safety requirements. Additional braking systems are mandatory e.g. for mainline vehicles, with travelling velocities > 140 km/h, in many countries, [1]. In this context, *mtb*s have proven to be effective since many years, [2], and their functionality at different adhesion conditions is validated by field investigations as well, [3].

When an *mtb*, shown in Fig. 1, is active, the electromagnets create magnetic attraction forces between brake and rail and occurring sliding friction forces in the *mtb*—rail contact are transmitted to the bogie. These braking forces increase with decreasing velocity, resulting in highest forces at the end of a braking manoeuvre. To avoid too high deceleration peaks at small velocities, called stopping jerks, *mtb*s were typically deactivated at $v_v < 20$ km/h. However, trends of increasing operational speed at unchanged infrastructure, put highest demands on the overall braking performance of railway vehicles and require *mtb* activation until full stop. First investigations of the stability and vibrational behaviour of an *mtb* in [4] reveal that the coupled electromagnetic-mechanical system is prone to self-excited vibrations at low velocities, which can be harmful to the mechanical structure. Two underlying phenomena causing self-excited

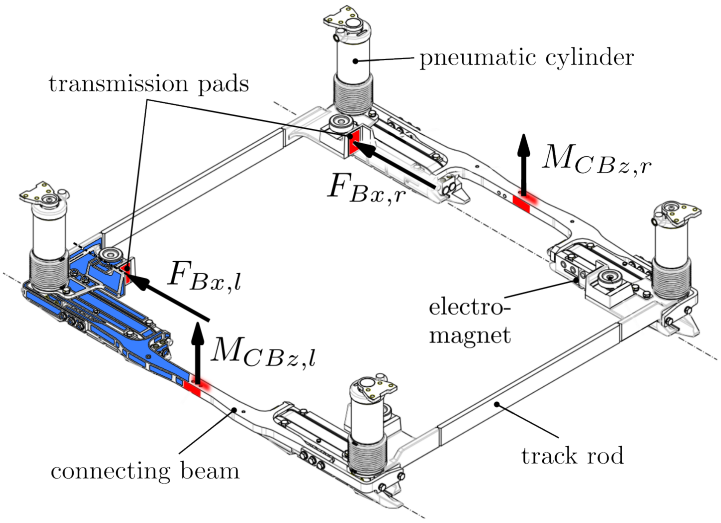

Figure 1. Main structure of an *mtb* with components, applied sensors (highlighted in red), and related measured loads at performed field tests.

vibrations were identified: 1. the coefficient of sliding friction, which increases with decreasing velocity, and is a known reason for self-excitations in other technical applications as well, and 2. the electromagnetic-mechanical coupling. It was shown that system parameters can be tuned, within reasonable limits, to get positive real parts of the eigenvalues of the linearized system, indicating a loss of asymptotic stability.

In [5] passive remedies to mitigate self-excited vibrations at *mtb*s and their positive influence were presented, but may not always be reasonable, because of constraints in the design or negative aspects regarding weight or braking performance. To overcome drawbacks from passive mitigations and to gain deeper system understanding, this paper presents first investigations on active vibration control at the coupled electromagnetic-mechanical system of an *mtb*, which is not addressed in literature so far. However, considerations at the related application of a basic friction oscillator are helpful here. In [6] the input of mechanical energy during one oscillatory period is studied to develop an active normal force control, able to diminish occurring self-excited vibrations.

Based on mentioned preliminary work, energy considerations are used to reveal influences of the self-excitation mechanisms and a new control law is obtained. The available electromagnet serves as the actuator and its electric voltage as the regulated variable of an implemented state feedback control. It is shown that the phase shift between magnetic and mechanical states can be controlled to force the system to dissipate more energy than it adds during each oscillation period. As a consequence, amplitudes may be reduced and vibrations may vanish.

The remainder of the paper is organized as follows. Section 2 presents the background of the underlying vibrational problem at *mtb*s. In section 3, the system model used for the investigation is shown. Section 4 presents the active control method and the implemented state feedback. In section 5 results of the active control, implemented on the non-linear system model, are depicted and in last section 6 conclusions and remarks for future research are given.

2. Background, measurements and preliminary results

To identify amplitudes and related load cycles at braking of an *mtb*, field tests until full stop were performed. Figure 1 shows the magnetic track brake used in the field tests. When the *mtb* is activated, the pneumatic cylinders mounted on the bogie move the track brake from the standby position onto the rail. During the activation process DC electric voltage is applied to the electromagnets at each corner, which are connected by track rods in lateral- and connecting beams in longitudinal direction, composing the brake frame. The powered

electromagnets generate a magnetic field, which is conducted by the pole shoes to the rail head and electromagnetic forces (EM forces) occur at the interfaces. EM forces are responsible for the main vertical forces in the *mtb*–rail contact, while the weight of the *mtb* and forces from the pneumatic cylinders are neglectable, [4]. Resulting frictional forces in the *mtb*–rail contact are transmitted by the brake frame towards the transmission pads, i.e. as braking forces $F_{B,i}$, into the bogie. Their longitudinal components, $F_{Bx,l}$ and $F_{Bx,r}$ see Fig. 1, were measured by force transducers during the field tests. Beside braking forces, bending moments around the vertical axis (z-axis) in the middle of the connecting beams, M_{CBzl} and M_{CBzr}, see Fig 1, are measured with applied strain gauges. Figure 2 depicts the measured signals during one braking manoeuvre, starting at approximately 100 km/h.

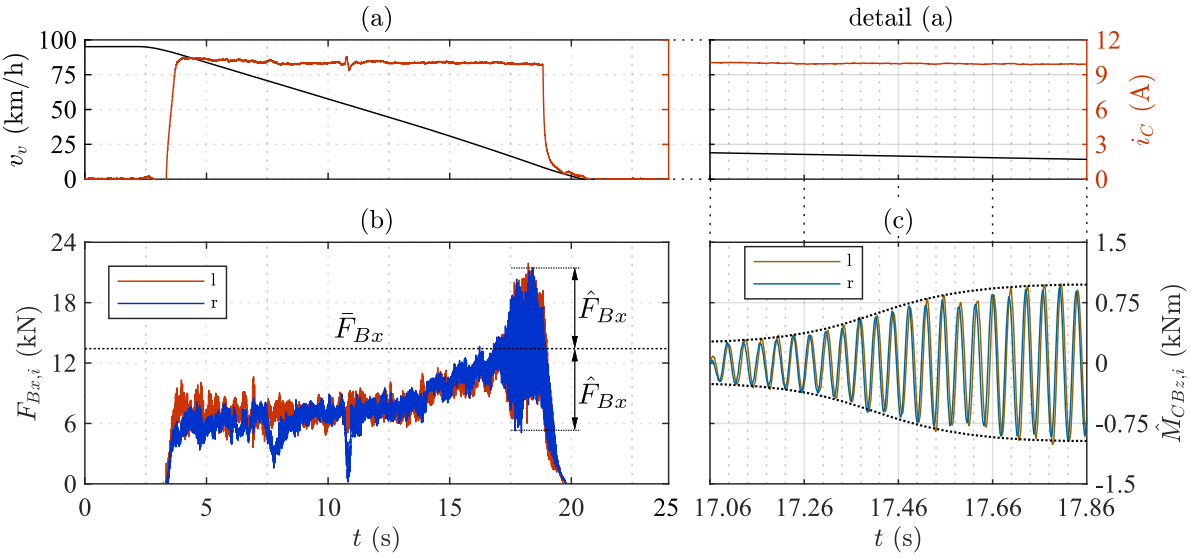

Figure 2. Measurements of a braking manoeuvre from 100 km/h to stand still, with the magnetic track brake active until $v_v \approx 8$ km/h.

Fig. 2 (a) depicts the measured vehicle velocity v_v and the electric current i_C, in the electric circuit of one electromagnet. The braking manoeuvre starts at approximately $t = 2.5$ s, indicated by the kink in the velocity signal, and ends when the vehicle is at stand still ($v_v = 0$ km/h) at roughly $t = 21$ s. The activation of the magnetic track brake is shown by the increasing electric current, which has a visible time delay, and the deactivation at $v_v \approx 8$ km/h is clearly indicated by the break down in the current signal. Diagram (b) in Fig. 2 depicts the related braking forces $F_{Bx,l}$ and $F_{Bx,r}$ of the *mtb* in the left and the right transmission link, respectively. The brake forces rise towards low velocities, which is expected because of the friction characteristic of the *mtb*–rail contact. The coefficient of sliding friction increases with decreasing velocity, while the gradient becomes even steeper at small velocities, [5]. At $v_v \approx 20$ km/h ($t \approx 17$ s), vibrations start to occur and amplitudes of the brake forces rise up to $\hat{F}_{Bx} \approx 8$ kN with a mean value of approximately $\bar{F}_{Bx} \approx 13$ kN and a frequency of $f_{osc} = 28.5$ Hz. These loads result in rather high stresses of the mechanical structure, combined with many load cycles, which may result in fatigue or even failure of the structure.

The right diagrams detail (a) and diagram (c) in Fig. 2 both depict a small time range of 0.8 s from the shown braking manoeuvre. Diagram (c) presents the amplitudes $\hat{M}_{CBz,l}$ and $\hat{M}_{CBz,r}$ of the measured bending moments $M_{CBz,l}$ and $M_{CBz,r}$. This figure reveals the behaviour of the occurring self-excited vibration, indicated by the dotted envelope. Starting with small

disturbances due to e.g. track irregularities, the amplitudes start to grow and after a short time span it reaches a maximum, indicating a limit cycle of the oscillating system. This behaviour is typical for non-linear systems, and well-known for friction induced self-excited vibrations, [7]. Additionally, it shows the oscillatory mode of this vibration. The amplitudes of the bending moments $\hat{M}_{CBz,l}$ and $\hat{M}_{CBz,r}$ at the opposite connecting beams are in phase while braking forces show a phase shift of 180°, which implies that the excited eigenmode of this vibration is an asymmetric mode with a measured frequency of 28.5 Hz. The mode was identified as the first asymmetric bending mode by FE-analysis in [5]. Detail (a) in Fig. 2 shows that the electric current i_C and the vehicle velocity v_v remain approximately constant during the amplitude increase of the bending moments in (c).
In [4] and [5] the stability behaviour of an *mtb* was studied for a simplified linearized quarter model, tuned to match the eigen-mode and frequency of the real system. Investigations with this model revealed two self-excitation mechanism as mentioned previously and were validated with a full system model. A full multibody model including all four magnets, electric circuits, suspension to the bogie and an elastic brake frame was used to simulate the whole braking manoeuvre and confirmed considerations of the simplified model. With the simplified linearized model passive mitigation methods were developed which worked for the full system model as well. Based on these findings, active mitigation methods discussed in this paper are developed with a similar quarter model, described in the following section 3 and the obtained control law, from section 4, is tested on the non-linear quarter model in section 5.

3. System model

The system model used in this paper consists of three coupled subsystems, describing a quarter of an *mtb*, similar to the model used in [4]. The electro-, magnetic-, and mechanical subsystems, shown in Fig. 3, are modelled with lumped parameters, while gray areas indicate the couplings in between.

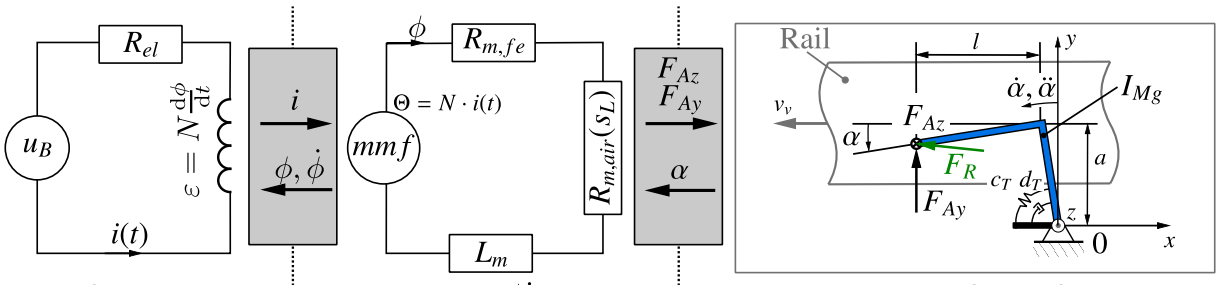

Figure 3. Lumped parameter model of the coupled electro-magnetic-mechanical system.

Mechanical subsystem: This subsystem, shown at the right of Fig. 3, is a planar 1 DOF (α) minimal model of a quarter magnetic track brake. It includes a rigid L-shaped body, highlighted in blue in Fig.1, with mass $m = 100$ kg, inertia $I_{Mg,0} = 2.25$ kgm², parameters $l = 0.34$ m and $a = 0.15$ m, and can rotate about the z-axis in fixed point 0 (transmission pad) to describe the motion of the identified mode shape. The torsional spring with stiffness c_T is tuned to match the same oscillatory frequency as measured at the field tests. The velocity proportional torsional damper, with damping constant d_T, represents the dissipative elements of the structure. While the transmission link with point 0 is fixed here, the rail below is moved with the vehicle velocity v_v, which is constant for these investigations. The contact between *mtb* and rail is considered in point A, which can slide on the moving rail in x and y direction, due to the rotation with

α. Electromagnetic forces in vertical and in lateral direction, F_{Az} and F_{Ay}, respectively the resulting friction force $F_R = F_{Az}\ \mu(v_{rel})$ are all applied in contact point A. The velocity dependent coefficient of sliding friction $\mu(v_{rel})$, with v_{rel} as the relative velocity between the rail v_v and the contact point velocity v_A, is linearized with respect to constant rail velocity v_v, with $\tilde{\mu} = \mu(v_v)$ and gradient k_μ of the μ - v characteristic. Neglecting small terms, the equation of motion reads:

$$I_{Mg,0}\ \ddot{\alpha} + d_T\ \dot{\alpha} + c_T\ \alpha = F_{Az}\ (\tilde{\mu} + k_\mu\ v_A)\ (a - \alpha l) - F_{Ay}\ (l + \alpha a) \tag{1}$$

Electric subsystem: This system covers the electric circuit of the electromagnet´s power supply. It consists of the provided DC voltage from the onboard battery, u_B, the electromotive force of the coil ϵ, which depends on the magnetic flux of the magnetic subsystem, and an electric resistance of the wiring and the coil's windings R_{el}. The output of this subsystem is the electric current i, responsible for the excitation of the magnetic field.
Magnetic subsystem: The magnetic subsystem is described by the shown magnetic equivalent circuit (MEC) in Fig. 3, frequently used in the modelling of mechatronic devices. The MEC consists of one exciting magnetomotive force (mmf) $\Theta = N\ i$, generated by the electromagnet's coil with N the number of windings, a magnetic resistance $R_{m,fe}$ of the iron involved (rail and pole shoes), the magnetic resistance of the air in between $R_{m,air} = \frac{s_L}{\mu_0\ A}$, varying with air gap s_L, having permeability μ_0 and cross section A, and an eddy current loss element $L_m = G\ \frac{\mathrm{d}\phi}{\mathrm{d}t}$ due to changing magnetic flux. The magnetic resistance of the iron parts is assumed to be constant. The differential equation describing the coupled electromagnetic system, [4], reads:

$$\dot{\phi} + \phi\ \frac{R_{m,fe} + \frac{s_L}{\mu_0 A}}{G R_{el} + N^2}\ R_{el} = u_B\ \frac{N}{G R_{el} + N^2} \tag{2}$$

The air gap is approximated by a hyperbolic function, based on magnetostatic analysis from [5]:

$$s_L = \frac{a_{hyp}}{b_{hyp}}\ \sqrt{b_{hyp}^2 + \alpha^2\ l^2} + 2z + a_{hyp0} \tag{3}$$

with parameters a_{hyp}, a_{hyp0}, b_{hyp} and the vertical distance z between magnet and rail.
The electromagnetic (EM) forces, acting on the mechanical system, can be derived from the partial derivative of the magnetic co-energy, [5], with lateral displacement from the middle of the rail head $y = l\alpha$:

$$F_{Az} = \frac{\phi^2}{2\mu_0 A}\ \frac{\partial s_L}{\partial z} = \frac{\phi^2}{\mu_0 A} \tag{4}$$

$$F_{Ay} = \frac{\phi^2}{2\mu_0 A}\ \frac{\partial s_L}{\partial \alpha}\ \frac{\partial \alpha}{\partial y} = \frac{\phi^2}{2\mu_0 A l}\ \frac{\partial s_L}{\partial \alpha} \tag{5}$$

Applied in (1) with $v_{Ax} = -\dot{\alpha}(a - \alpha l)$ as velocity of contact point A in $x-$direction, one obtains for the mechanical system:

$$I_{Mg,0}\ \ddot{\alpha} + d_T\ \dot{\alpha} + c_T\ \alpha = \frac{\phi^2\ \tilde{\mu}}{\mu_0 A}(a - \alpha l) - \frac{\phi^2\ k_\mu}{\mu_0 A}\dot{\alpha}(a - \alpha l)^2 - \frac{\phi^2\ (l + \alpha a)}{2\mu_0 A l}\ \frac{\partial s_L}{\partial \alpha} \tag{6}$$

The coupled electromagnetic-mechanical system described by (2) and (6), can be written in a system of three non-linear inhomogeneous ODE with the state vector: $\boldsymbol{x} = [\alpha\ \dot{\alpha}\ \phi]^T$.

4. Active Mitigation

At self-excited vibrations the necessary energy to compensate dissipation losses is drawn from an available energy source by the motion itself, which results in growing amplitudes until an energy balance is reached, [7]. This consideration can be used for mitigation measures as well, i.e. the energy input must be smaller than the dissipation losses which directly reduces occurring amplitudes, used e.g. in [6]. The input of mechanical energy drawn and dissipated by the motion during one oscillating period is derived:

$$\Delta E_P = \int_0^T \left(\boldsymbol{F}_R \cdot \boldsymbol{v}_A + \boldsymbol{F}_{Ay} \cdot \boldsymbol{v}_A - d_T \, \dot{\alpha}^2 \right) \mathrm{d}t \tag{7}$$

with the vector $\boldsymbol{v}_A = -\dot{\alpha} \left[(a - \alpha l) \cdot \boldsymbol{e}_x + (l + \alpha a) \cdot \boldsymbol{e}_y \right]$ as the velocity of the contact point A. A system with small amplitudes with respect to the quasi-steady-state $StSt$ is assumed. The $StSt$ is derived by (2) and (6) using $\alpha = \alpha_0$, $\dot{\alpha} = 0$, $\phi = \phi_0$, $\dot{\phi} = 0$. To study the energy input on the simplified system, each term in (7) is linearized with respect to the $StSt$ and integrated over one oscillation period. Linearized EM forces are derived from (4) respectively (5)

$$F_{Azlin} = F_{Az|StSt} + \left(\frac{\partial F_{Az}}{\partial \phi} \right)_{|StSt} (\phi - \phi_0) \tag{8}$$

$$F_{Aylin} = F_{Ay|StSt} + \left(\frac{\partial F_{Ay}}{\partial \phi} \right)_{|StSt} (\phi - \phi_0) + \left(\frac{\partial F_{Ay}}{\partial \alpha} \right)_{|StSt} (\alpha - \alpha_0) \tag{9}$$

and

$$F_{Rlin} = F_{Azlin} \left(\tilde{\mu} - k_\mu \left(\dot{\alpha} \, (a - \alpha_0 \, l) \right) \right) \tag{10}$$

Figure 4 depicts the behaviour of the linearized system during one oscillation period. States $\dot{\alpha}$ and ϕ with respect to their quasi-steady-states are shown in (a) and (b).

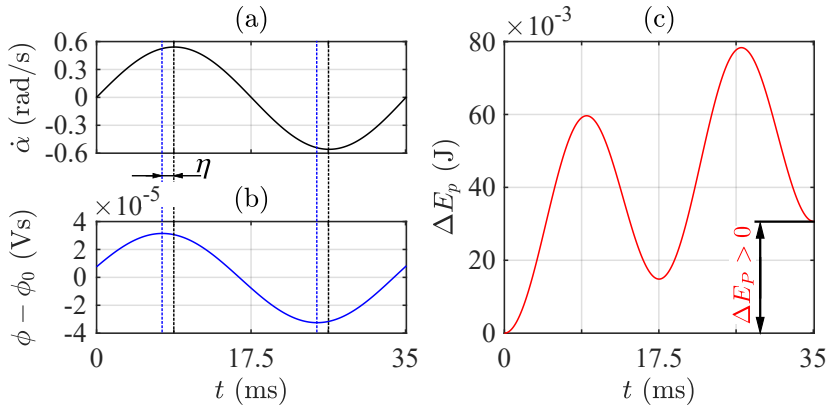

Figure 4. Angular velocity $\dot{\alpha}$ (a), magnetic flux ϕ (b) and energy input ΔE_p (c) during one oscillation period T.

The related energy during this period, calculated numerically, is shown in Fig. 4 (c). $\Delta E_P > 0$ implies that the system draws more energy from the coupled electromagnetic system and the frictional contact during the oscillation period than it dissipates. Hence, amplitudes will grow over time finally resulting in a stable limit cycle. The magnetic flux in figure 4 (b) oscillates with the frequency of the mechanical state, Fig. 4 (a). As shown in the diagrams, the magnetic flux

leads the mechanical motion by the phase shift η depending on the chosen model parameters of the electromagnetic system (2).
For possible mitigation methods, the energy defined in eq. (7) must become negative to reduce occurring amplitudes. All considered forces depend on the magnetic flux ϕ while their contact point, A, oscillates with the mechanical state variable $\dot{\alpha}$, see eq. (8)-(10). This implies a coupling of the magnetic state variable ϕ and the mechanical state $\dot{\alpha}$ in (7). After loss of stability the oscillating states are assumed to be harmonic functions. Then, the magnitude of coupling term $C_{\phi,\dot{\alpha}}$, becomes smaller for increasing phase shifts between the considered states. Beside $C_{\phi,\dot{\alpha}}$, terms with the mechanical states appear. Without undesirable changes of the quasi-steady-state, they can not be affected by the available actuator directly, but are reduced as a consequence of the mitigation method.
In the scope of this paper the possibility of an active control, which is able to force the phase shift to a specific value $\eta = \pi$, by modulating the electric voltage supply $u_B = u_B(t) = u_{B0} + \Delta u_B(t)$, is investigated. With the aim of a negative energy balance $\Delta E_P < 0$, based on reduced electromagnetic-mechanical coupling terms, emerging amplitudes may decrease after loss of stability and activation of electric voltage modulation. From linearization of (2) the modulated electric voltage follows:

$$\Delta u_B = \frac{1}{K_{u,ODE1}} \left(\Delta\dot{\phi} + \left(\frac{\partial K_{\phi,ODE1}}{\partial \alpha} \right)_{|StSt} \Delta\alpha + \left(K_{\phi,ODE1} \right)_{|StSt} \Delta\phi \right) \tag{11}$$

with variables $K_{\phi,ODE1} = (R_{m,fe} + \frac{s_L(\alpha)}{\mu_0 A}) R_{el} / (GR_{el} + N^2)$ and $K_{u,ODE1} = N/(GR_{el} + N^2)$. For a specific phase shift of $\eta = \pi$, the assumed harmonic behaviour of the mechanical state $\dot{\alpha} = \hat{\dot{\alpha}}\ sin(\omega t)$ and $\alpha = \alpha_0 - \hat{\alpha}\ cos(\omega t)$ is used to describe the magnetic state ϕ:

$$\Delta\phi = -\hat{\phi}\ sin(\omega t) = -\frac{\hat{\phi}}{\hat{\alpha}} \frac{1}{\omega}\ \Delta\dot{\alpha} \tag{12}$$

$$\Delta\dot{\phi} = -\hat{\phi}\ \omega\ cos(\omega t) = \frac{\hat{\phi}}{\hat{\alpha}}\ \omega\ \Delta\alpha \tag{13}$$

with the eigenfrequency ω of the closed loop system. With (11) the control law for the modulated voltage to reach the predetermined phase shift $\eta = \pi$ is derived to

$$\Delta u_B = -\boldsymbol{K} \cdot [\Delta\alpha, \Delta\dot{\alpha}, \Delta\phi]^T \tag{14}$$

$$\boldsymbol{K} = \frac{1}{K_{u,ODE1}} \left[-\frac{\hat{\phi}}{\hat{\alpha}}\ \omega - \left(\frac{\partial K_{\phi,ODE1}}{\partial \alpha} \right)_{|StSt},\ \frac{\hat{\phi}}{\hat{\alpha}} \frac{1}{\omega} \left(K_{\phi,ODE1} \right)_{|StSt},\ 0 \right]^T \tag{15}$$

If the quasi-steady-state is known and the eigenfrequency Ω of the open loop system identified, assuming $\omega \approx \Omega$, a state feedback controller with gain factor $k = \hat{\phi}/\hat{\alpha}$ to reduce the effective input energy, based on the electromagnetic-mechanical coupling terms, is found. Figure 5 depicts the behaviour of the linearized system with the active state feedback. The magnetic flux (b) shows the desired phase shift of $\eta = \pi$ to the angular velocity $\dot{\alpha}$, shown in diagram (a). The calculated energy during the shown oscillating period is negative $\Delta E_{P,lin} < 0$ resulting in decreasing amplitudes and terminated self-excitation.

5. Results

The control law from section 4, developed with the linearized system model, will now be applied for active mitigation of self-excited vibrations to the non-linear system model of section 3. Input of the controller is the state space vector $\Delta x = [\alpha - \alpha_0, \dot{\alpha}, \phi - \phi_0]^T$, with known quasi-steady-states. Figure 6 depicts the time simulation of the mechanical state α at the upper diagrams and

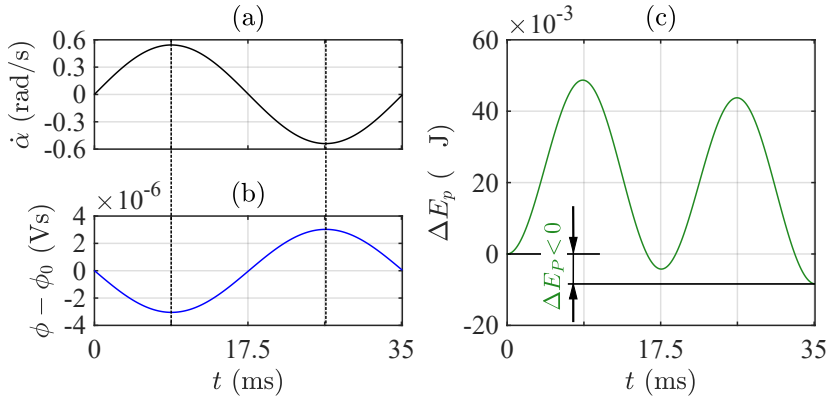

Figure 5. Angular velocity $\dot{\alpha}$ (a), magnetic flux $\phi - \phi_0$ (b), energy input $DeltaE_P$ (c) during one oscillation period with implemented controller for gain factor $k = 1$ mVs/rad, of the linearized system.

the related modulated voltage at the lower ones, for different gains k. The controller is activated at $t = 1$ s. Starting at the stable limit cycle of the non-linear system, the oscillation amplitudes decrease and the state variables decay to their quasi-steady-states. The state feedback control is able to diminish already developed oscillations of the non-linear system. By changing the phase shift without altering quasi-steady-states, loss in braking power is kept small.

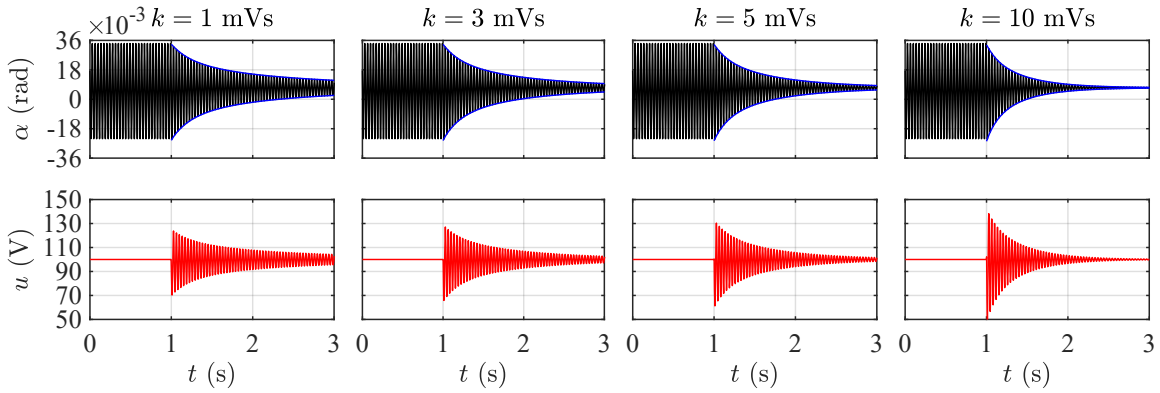

Figure 6. Mechanical state $\alpha(t)$ and related electric voltage $u(t)$ of the non-linear system model with the active control, activated at $t = 1$ s for different gains k.

With increasing gains k, the time constants τ_k characterising the envelope $\exp(-\frac{t}{\tau_k})$ of the decreasing mechanical oscillation decrease and the voltage amplitudes of the control input increase. In Table 1 the related time constants τ_k, the maximum amplitudes of the electric voltages $\hat{u}_{max,k}$, which occurs when the controller is activated, for different gains k of Fig. 6, and their ratio with respect to the values at $k = 1$ mVs, τ_k/τ_1 and $\hat{u}_k/\hat{u}_1$, are listed. The electric energy, necessary for the demanded gains $k = \hat{\phi}/\hat{\alpha}$, increases with reduced time constants τ_k. While the necessary voltage amplitudes are rising linearly with applied gain, (15), the related time constants show a degressive, almost hyperbolic decline with increased gains, $\tau_k \propto \left(\frac{C_1}{C_2+k} + C_3\right)$. From $k = 1$ to $k = 3$, the voltage amplitudes are increased by ≈ 4.6 V, while the time constant is reduced by 0.46 s. The increase in voltage amplitudes is similar from $k = 3$ to $k = 5$, but results in a reduction of the time constant of 0.2 s, which is significantly smaller. Hence, the cost in voltage supply are rising for the same benefit of reduced time at higher gains. For practical implementation an optimum between short time constants and necessary voltage supply should be found. However, each gain applied, is able to diminish the oscillation of the

Table 1. Time constant τ_k, ratio of the time constants τ_k/τ_1, necessary voltage amplitude when the controller is activated $\hat{u}_{max,k}$, and the related ratio $\hat{u}_{max,k}/\hat{u}_{max,1}$, related to Fig. 6.

k, (mVs/rad):	1	3	5	10
τ_k, (s)	1.27	0.81	0.61	0.38
τ_k/τ_1, (1)	1.00	0.64	0.48	0.30
$\hat{u}_{max,k}$, (V)	29.6	34.2	38.7	50.2
$\hat{u}_k/\hat{u}_1$, (1)	1.00	1.15	1.31	1.70

non-linear system with a higher input of electrical energy (voltage) resulting in shorter time constants and therefore reduced mechanical loads of the structure.

6. Conclusion and Outlook

Field tests have shown that a magnetic track brake is prone to harmful self-excited vibrations at low velocities. Measurements during braking manoeuvres revealed the eigen-mode and frequency of the oscillations and a respective limit cycle. Within this paper, a quarter model of the magnetic track brake was used to investigate a new active control method of the electric voltage supply to diminish occurring oscillations. The applied lumped parameter model of the electromagnetic subsystem, is coupled to a mechanical subsystem which can oscillate on a moved rail with constant velocity. A state feedback control with the electric voltage as the regulated variable, is developed to reach a specific phase shift between magnetic flux and the mechanical motion, which results in a negative energy balance during one oscillation period. Hence, oscillating amplitudes are reduced and in further consequence the vibration diminishes.
However, the developed controller should be investigated on a more detailed *mtb*-model, considering that the states may not all be measured and a state observer may be required. Within this model the real electric wiring of the different magnets must be considered. The influence of changing operation conditions, e.g. friction conditions should be studied with respect to the necessary voltage amplitude. For large gains k the assumed linear material behaviour must be validated before practical implementation as well.

Acknowledgments

The financial support by the Austrian Federal Ministry for Digital and Economic Affairs, the National Foundation for Research, Technology and Development and the Christian Doppler Research Association is gratefully acknowledged.

References

[1] International Union of Railways 2014 *UIC-Kodex 546 Vorschriften für den Bau der verschiedenen Bremsteile - Hochleistungsbremsen für Personenzüge* (Paris: UIC) p.8
[2] Gfatter G, Haas S, Vohla G 2004 *Schienenbremsen/track brakes* vol 1 (Munich: Knorr-Bremse GmbH) p.138
[3] Arias-Cuevas O, Li Z 2012 Field investigations into the performance of magnetic track brakes of an electrical multiple unit against slippery tracks Part 2: Braking force and side effects *Proc IMechE Part F: J Rail and Rapid Transit* **226(1)** 72-94
[4] Tippelt D, Edelmann J, Plöchl M, Jirout M 2019 Analysis of Self-excited Vibrations of an Electromagnetic Track Brake *Advances in Dynamics of Vehicles on Roads and Tracks IAVSD* 12-16
[5] Tippelt D, Edelmann J, Plöchl M, Jirout M 2021 Modelling, analysis and mitigation of self-excited vibrations of a magnetic track brake *Proc IMechE Part F: J Rail and Rapid Transit* **236(6)** 684-694
[6] Popp K, Rudolph M 2004 Vibration Control to Avoid Stick–Slip Motion *J of Vibration and Control* **10** p.16
[7] Den Hartog JP 1985 *Mechanical vibrations* vol 4 (New York: Dover Publications) p.342